

Solving Boolean Satisfiability Problems Using A Hypergraph-based Probabilistic Computer

Yihan He^{1†}, Ming-Chun Hong^{2,3†}, Wanli Zheng¹, Ching Shih^{2,3}, Hsin-Han Lee³, Yu-Chen Hsin³, Jeng-Hua Wei³, Xiao Gong¹, Tuo-Hung Hou^{2,4}, and Gengchiau Liang^{1,4*}

¹Department of Electrical and Computer Engineering, National University of Singapore, 117583 Singapore

²Department of Electrical Engineering and Institute of Electronics, National Yang-Ming Chiao Tung University, Hsinchu, Taiwan

³Electronic and Optoelectronic System Research Laboratories, Industrial Technology Research Institute, Hsinchu, Taiwan

⁴Industry Academia Innovation School, National Yang-Ming Chiao Tung University, Hsinchu, Taiwan

[†]These authors contribute equally; *Email: geliang@nycu.edu.tw

Boolean Satisfiability (SAT) problems are critical in fields such as artificial intelligence and cryptography, where efficient solutions are essential. Conventional probabilistic solvers often encounter scalability issues due to complex logic synthesis steps. In this work, we present a novel approach for solving the 3-SAT Boolean satisfiability problem using hypergraph-based probabilistic computers obtained through direct mapping. This method directly translates 3-SAT logical expressions into hypergraph structures, thereby circumventing conventional logic decomposition and synthesis procedures, and offering a more streamlined solver architecture. For a uf20-01 instance, our approach significantly reduces the vertex number from 112 to 20 with a reduced solution space from 2^{112} to 2^{20} . Numerical simulations demonstrate that the proposed hypergraph-based solver achieves a significantly higher success rate of up to 99%, compared to merely 1% for conventional solvers. Furthermore, the proposed direct mapping method can be extended to solve k-SAT problems, which provides a scalable framework for tackling more complex satisfiability problems using probabilistic computing in the future.

Introduction

In recent years, probabilistic computing based on probabilistic bit (p-bit)^{1–7} has been recognized as an unconventional computing paradigm in response to the diminishing returns of classical deterministic computing, particularly as the benefits of Moore’s Law plateau. By leveraging the inherent randomness in physical systems, probabilistic computing enables computations based on probability distributions rather than fixed binary states. A particularly promising application of probabilistic computing is combinatorial optimization problems (COPs)^{8–12}, where classical computers struggle with scalability and efficiency. Based on the architecture of simple undirected graphs (SUGs), probabilistic computers constructed from Boltzmann machines (BMs)^{10,13–15} or the Ising model^{3,16–18} demonstrate superior capabilities in solving hard computational problems with vast solution space. Among these, the Boolean Satisfiability (SAT) problem¹⁹, particularly the 3-SAT variant, stands out due to its wide

applications in artificial intelligence²⁰, electronic design automation²¹, and cryptography²². The 3-SAT problem seeks to determine a variable assignment that satisfies a Boolean formula composed of clauses, each containing exactly three literals.

Current probabilistic solvers based on invertible logic for SAT problems often rely on logic synthesis methodologies^{23–25}, as shown in **Fig. 1(a)**. These approaches initially construct small SUGs capable of implementing basic logical functions from the truth tables²⁶ or logical expressions of target logic gates²⁷. Common examples include invertible NOT (INOT), invertible OR (IOR), and invertible AND (IAND) gates. Then these independent SUGs can be combined according to pre-designed logic diagrams to form larger-scale combinatorial invertible logic circuits to solve SAT problems. However, this approach faces great challenges in scalability. In a 3-SAT problem, each clause contains three variables, which is typically realized in the graph by two merged SUGs of IOR gates. This produces an auxiliary vertex for each clause. As the scale of 3-SAT problems increases, the growing number of clauses introduces a substantial number of similar auxiliary vertices. This proliferation of auxiliary vertices significantly increases the overall node overhead, exacerbates the structural complexity of the graph by enhancing connectivity and depth, and complicates the energy landscape of the system. Additionally, the exponential growth of the solution space places considerable demands on the solver’s computational capabilities and hardware resources. Consequently, solvers encounter severe performance bottlenecks when addressing large-scale 3-SAT problems.

To address these limitations, recent research has explored the incorporation of higher-order or many-body interactions among vertices^{16,28–30}. Studies have demonstrated that higher-order bipolar Ising machines, implemented with coupled oscillators^{16,31} or CMOS spin systems³², can find solutions more efficiently with fewer spin variables, i.e. less vertex overhead, compared to conventional second-order Ising machines. However, a critical limitation of this scheme is the deterministic representation of spin variables. It impedes the system’s ability to escape local energy minimum points once trapped, thereby compromising the quality of solution and overall accuracy. As a result, a careful and appropriate design of annealing schedules is indispensable for ensuring convergence to the global optimum³³.

In light of these challenges, inspired by a reconfigurable deterministic Ising machine with direct mapping³², we present a novel probabilistic computing approach based on invertible logic developed from BMs. Employing binary variable representation, the proposed design methodology can directly map 3-SAT logical expressions onto hypergraph structures (**Fig. 1b**), rather than merging SUGs. This design cleverly circumvents the intrinsic logic decomposition and synthesis procedures embedded in conventional probabilistic SAT solvers. Such a direct mapping technique offers three key advantages: (1) minimizing vertex overhead, (2) simplifying the structural complexity of the solver, and (3) achieving the theoretically minimal solution space. Meanwhile, the core of our probabilistic solver lies the Boltzmann distribution (**Fig. 1c**), which governs the stochastic sampling of state configurations according to their energy. To further improve the solution quality, we also incorporate simulated annealing by dynamically increasing the system’s stochasticity level parameter to facilitate the system to converge toward the global optimum (ground state). By leveraging the natural randomness of p-bit devices and the annealing-enhanced Boltzmann sampling process, our solver demonstrates significantly improved success rates and computational efficiency on practical 3-SAT instances.

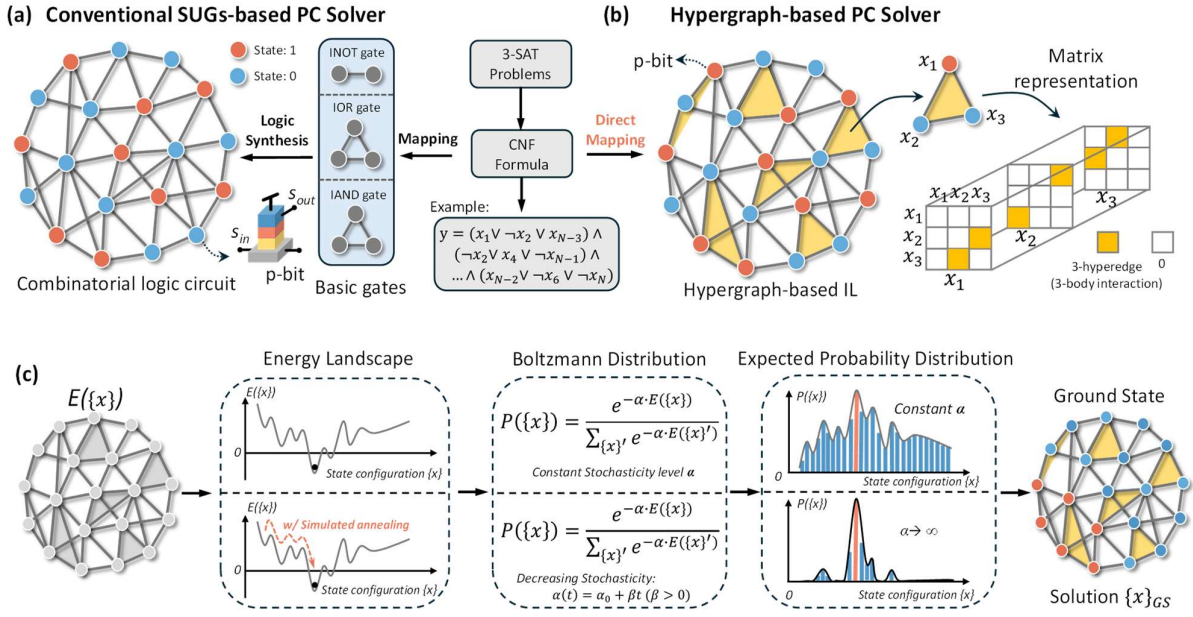


Fig. 1 Comparative illustration of conventional and proposed hypergraph-based probabilistic computing approaches for solving the 3-SAT problem. (a) Conventional probabilistic SAT solvers constructed from merged SUGs. These solvers typically synthesize basic invertible logic gates, including INOT, IOR, and IAND gates to form a combinatorial probabilistic solver. Vertices represent binary variables and are implemented with p-bit devices. Pairwise interactions among vertices are depicted by black lines. (b) The proposed solver based on direct mapping from conjunctive normal form (CNF) logical expressions to hypergraph structures. Each hyperedge in yellow-colored region represents higher-order interactions involving multiple vertices, corresponding directly to the clauses within a 3-SAT problem. (c) Underlying physical mechanisms of solving the SAT within probabilistic computing paradigm. The probabilistic dynamics of the proposed system are governed by the Boltzmann distribution, where the probability of a state configuration $\{x\}$ depends on its energy $E(\{x\})$ and real-time stochasticity level α of the system. To enhance convergence, simulated annealing is also employed, which gradually sharpens the sampling distribution toward the ground state.

Results

A. Direct mapping 3-SAT to hypergraphs

The core of solving 3-SAT problems based on probabilistic computing resides in the formulation of an appropriate energy function that accurately represents the objective function or logical expression. This process must ensure that the optimal solution, which may correspond to one or multiple variable assignments, of the problem to be solved is mapped to the ground state of the system's energy landscape. The universally applicable mapping methodology we developed allows the direct construction of invertible logic-based probabilistic solvers for 3-SAT utilizing energy models based on hypergraph structures. This approach is also designed to be scalable, which can be extended to higher-order k -SAT problems, thus offering a versatile framework for broader applicability in complex SAT problem domains.

The formula of a 3-SAT problem is expressed as a conjunction (logical AND) of m clauses, each containing exactly three literals (variables or their negations) connected by disjunctions

(logical OR). Formally, the general form of the 3-SAT problem can be represented as follows:

$$(x_1 \vee \neg x_2 \vee x_{N-3}) \wedge (\neg x_2 \vee x_4 \vee \neg x_{N-1}) \wedge \dots \wedge (x_{N-2} \vee \neg x_6 \vee \neg x_N) \quad (1)$$

where N denotes the total number of variables.

The objective of the 3-SAT problem is to find a combination of true or false assignments for the variables x_1, x_2, \dots, x_N , that makes the entire formula true, which is a canonical NP-complete problem. To address the problem using our approach, we begin by defining an encoding rule that uniformly represents both positive and negative literals in a binary format. Specifically, the encoding of literals is given by:

$$x_i \rightarrow (1 - x_i) \quad (2a)$$

$$\neg x_i \rightarrow x_i. \quad (2b)$$

This encoding allows us to equally handle the literals within each clause. Applying the encoding from Eq. (2), we can derive individual energy functions for each clause:

$$\begin{aligned} H_1 &= (1 - x_1) \cdot x_2 \cdot (1 - x_{N-3}) \\ H_2 &= x_2 \cdot (1 - x_4) \cdot x_{N-1} \\ &\vdots \\ H_m &= (1 - x_{N-2}) \cdot x_6 \cdot x_N \end{aligned} \quad (3)$$

where each energy function H_i represents a product of terms corresponding to the encoded literals. This reflects the constraints imposed by the disjunctions within each clause. The overall energy landscape of the 3-SAT problem can be obtained by summing the energy functions of all m clauses. Therefore, the total energy function H_{total} for the entire 3-SAT problem is expressed as:

$$H_{total} = \sum_{i=1}^m H_i == \sum W_{ijk} \cdot x_i x_j x_k + \sum J_{ij} \cdot x_i x_j \sum h_i \cdot x_i + \dots + C \quad (4)$$

where W_{ijk} , J_{ij} and h_i represent the coefficients for hyperedges, pairwise interactions, and biases respectively, and C is a constant term. These parameters directly correspond to the coefficients of the hypergraph.

The summation operation of each energy function encapsulates the collective constraints imposed by the conjunction of all clauses. Using this approach, the system reaches its ground state, namely $H_{total} = 0$, only when the variables x_1, x_2, \dots, x_N are assigned in such a way that the entire formula is satisfied, i.e., evaluates to true. Any other assignments of variables that do not satisfy the formula will return a total energy H_{total} greater than zero.

Following the outlined mapping procedure, **Fig. 2(a)** presents an example of a 3-SAT problem consisting of five literals and three clauses. In its direct mapping to a hypergraph depicted in **Fig. 2(b)**, each variable is represented as one vertex, while the constraints between clauses and the relationships between literals within a clause are fully captured by hyperedges, pairwise interactions, and bias terms.

B. Improved SUGs-based logic synthesis

We also prepared the conventional approach of constructing 3-SAT solvers using SUGs derived from the logic synthesis of basic gates. However, we made several specific improvements to prior conventional methods^{25,34}, which typically rely on combining SUGs for INOT, IOR, and IAND gates. The presence of INOT gates is required to represent negated literals in the logical formulation. Later, in the logic synthesis process, the output vertex of the NOT gate's SUG needs to merge with one of the input nodes of the IOR gate, which introduces an additional auxiliary node.

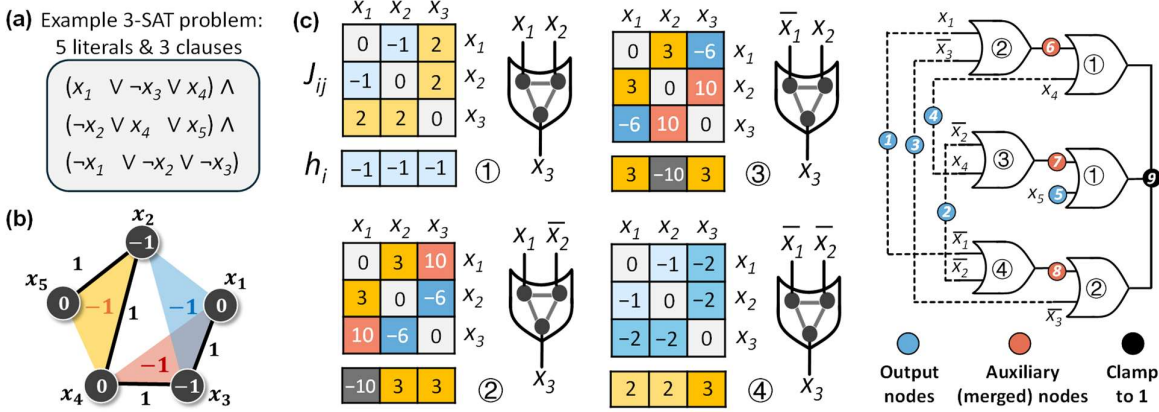


Fig. 2. (a) Example small-scale 3-SAT problem with 5 literals and 3 clauses. (b) Hypergraph representation of the 3-SAT problem after direct mapping. Hyperedges are illustrated by three colored regions: red, yellow and blue, respectively. Pairwise interactions between vertices are depicted by black lines. The strength of hyperedges and pairwise interactions are indicated by the numbers adjacent to the regions and lines. Local bias term and its strength are represented as white numbers within the vertices. (c) Four types of IOR gates utilized in SUGs-based probabilistic 3-SAT solvers. Each IOR gate is defined by a pairwise interaction matrix J_{ij} and an external bias vector h_i . In conventional SUG-based solvers, these IOR gates undergo logic synthesis and merge shown as the diagram on the right-hand side. Output nodes (blue), auxiliary merged nodes (orange), and nodes clamped to logical “1” (black) collectively define the resulting densely interconnected probabilistic network.

To address this issue, we designed individual OR gate SUGs for the four possible input-output relationships of each clause in the 3-SAT problem, namely $x_3 = x_1 \vee x_2, x_3 = x_1 \vee \neg x_2, x_3 = \neg x_1 \vee x_2$, and $x_3 = \neg x_1 \vee \neg x_2$. **Fig. 2(c)** illustrates the detailed matrix representations of these IOR gate SUGs, explicitly showing the pairwise interaction matrix J_{ij} and external bias matrix h_i . The matrix elements represent the interaction strength between corresponding nodes, where color coding differentiates positive, negative, and zero interactions. The right-hand side demonstrates how these optimized gate designs are merged during the logic synthesis procedure for this simple instance. The black node is clamped to logic “1” to ensure correct logic behavior. The output nodes in blue are the source of the signals we observe, and the auxiliary nodes in orange are generated during the logic synthesis process.

Through this refined design, the node overhead of solvers constructed by conventional methods can be minimized, reducing the overall complexity of the system and avoiding potential negative impacts on efficiency. This optimization ensures a fair performance comparison in the subsequent section between the conventional and our proposed hypergraph-based method, as the best version of the conventional approach is used for benchmarking.

C. Tunable p-bit devices and systems

The implementation of p-bit device is various, including but not limited to magnets-based^{4,35,36}, memristors^{8,37,38}, FPGA^{14,14,39}, and ferroelectric transistors⁴⁰. In this work, we adopted a stochastic spin-transfer torque magnetic random access memory (STT-MRAM)⁴¹ as a tunable p-bit device. The cross-sectional TEM image in **Fig. 3(a)** shows its layered composition. This

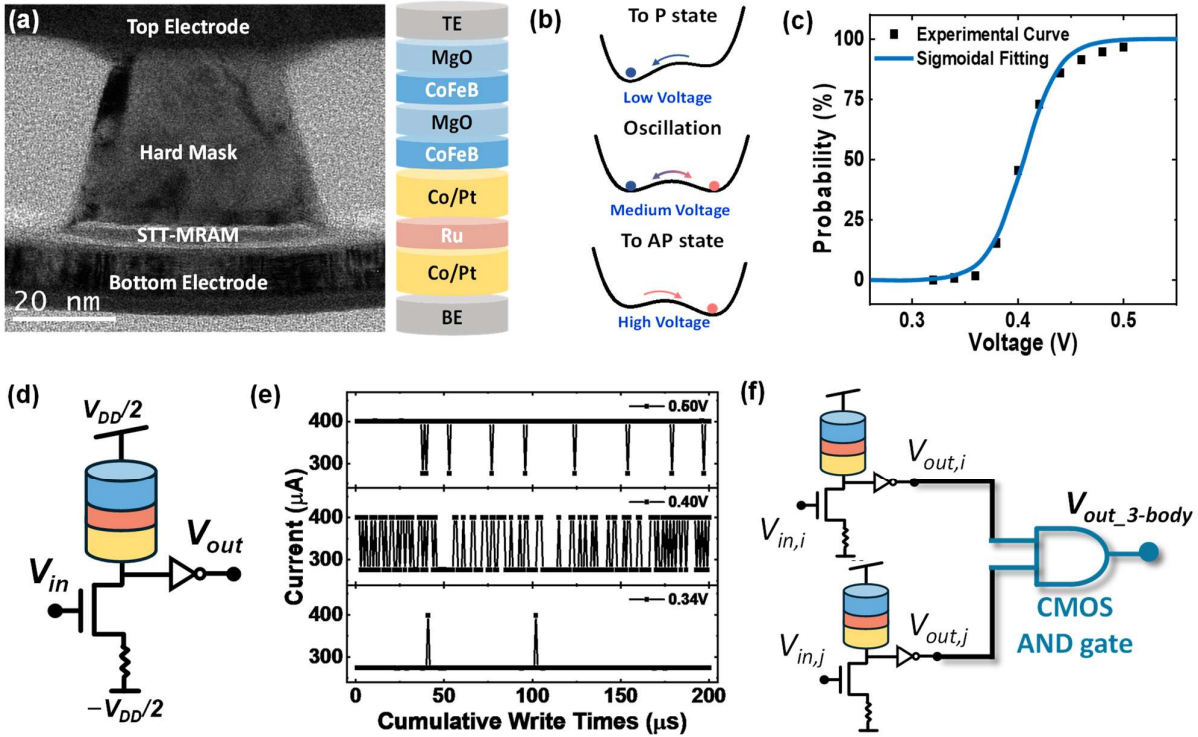


Fig. 3. (a) Cross-sectional TEM image of a Spin-Transfer Torque Magnetic Random-Access Memory (STT-MRAM) structure. The labeled layers include the Top Electrode (TE), MgO barrier, CoFeB free and fixed layers, Co/Pt multilayers, Ru spacer, and Bottom Electrode (BE). (b) Voltage-dependent switching behavior of the STT-MRAM. (c) Output probability versus voltage characteristics of the magnetic tunnel junction, presenting experimental data (black dots) alongside the sigmoidal fitting curve (blue line). The fitting curve was used in subsequent simulations for solving the 3-SAT problems. (d) Schematic representation of the stochastic STT-biased p-bit device (e) State fluctuation over time under varying input voltages, representing the tunable stochasticity of the tunable p-bit device. (f) Prospective hardware of a conventional CMOS AND gate for implementing three-order interactions in binary output systems.

device demonstrates distinctive switching characteristics across various voltage ranges: at a low applied voltage, the device stabilizes in the “AP state” (antiparallel state), whereas high voltage conditions drive it into the “P state” (parallel state)⁴¹. Within an intermediate voltage range, the device enters a tunable oscillation regime. As shown in **Fig. 3(b)**, it fluctuates between the “P” and “AP” states. This voltage-dependent oscillation under medium voltage conditions is central to the device’s operation as a tunable p-bit device. The stochastic behavior of the device is experimentally characterized in **Fig. 3(c)**, where the observed data (black squares) conform closely to a sigmoidal fitting curve (blue line), illustrating a smooth probabilistic transition between states in response to varying input voltage. This sigmoidal response is essential for achieving the tunable probabilistic output required for the probabilistic computing applications considered in this study. **Fig. 3(d)** shows the basic circuit configuration of the STT-biased probabilistic device. The temporal behavior of the device current under different bias voltages is further shown in **Fig. 3(e)**. In our further modeling and system-level simulations in solving the 3-SAT problems, we extracted this

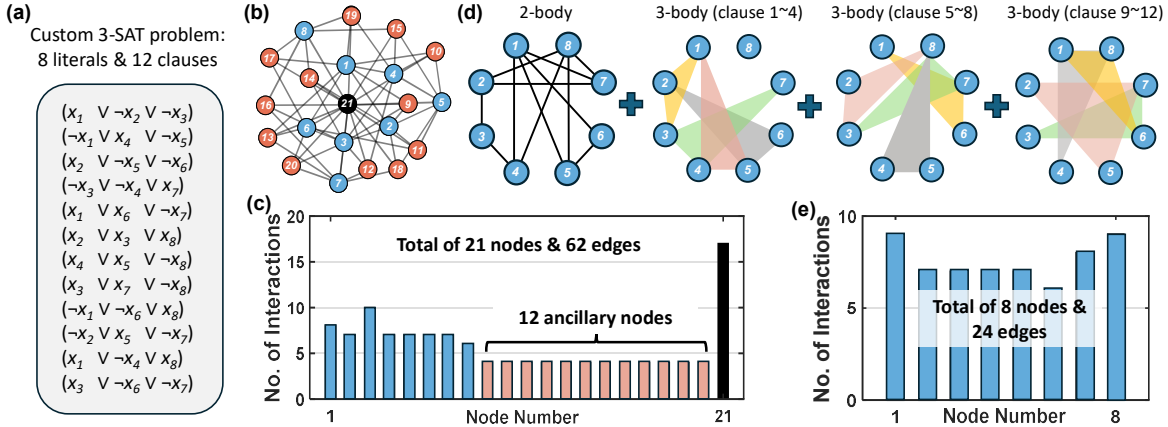


Fig. 4. (a) Custom-defined 3-SAT problem utilized for evaluating solver performance, with clauses interconnected through logical conjunction. (b) Graphical representation and (c) node-interaction distribution of a conventional 3-SAT solver constructed using the logic synthesis method based on optimized SUGs. (d) Direct hypergraph-based mapping for the same 3-SAT problem. For better visualization, hyperedges for the 12 clauses are divided into three parts and presented respectively with colored regions enclosing multiple vertices. (e) Node and edges distribution of the 3-SAT solver based on the direct mapping method.

sigmoidal curve and encapsulated it into a cell with a probability of 50% to get 0 or 1 at $V = 0$. Moreover, to represent the involved three-order interactions of binary states in hypergraphs, we employed standard CMOS AND gates, as shown in **Fig. 3(f)**. This electronic element could serve as a hardware implementation of hyper-degree (three-body) interactions when the system evolves. It provides a simple potential solution for implementing probabilistic networks based on hypergraphs.

D. Numerical simulation on various 3-SAT instances

To evaluate the performance of the proposed hypergraph-based direct mapping method in comparison with the optimized logic synthesis approach, a customized 3-SAT instance was analyzed as an initial case study. As shown in **Fig. 4(a)**, this instance is composed of 8 literals and 12 clauses with 28 valid satisfying assignments. This instance presents a slightly complex yet measurable test case. **Fig. 4(b)** presents the merged SUGs that use the optimized conventional approach. This configuration totally comprises 21 vertices. Vertex 21 is connected to all other vertices and is clamped to a state of 1 to enforce correct solution constraints. Vertices 1 to 8 serve as output terminals from which the statistics are collected. Vertices 9 to 20 act as 12 auxiliary nodes. These auxiliary nodes emerge from the logic synthesis process, specifically from the merging of two IOR gates per clause. From the perspective of structural complexity, this network exhibits a high density of connections, consisting of 62 pairwise edges that interconnect throughout the SUG (**Fig. 4c**). In contrast, the hypergraph-based solver derived through direct mapping is depicted in **Fig. 4(d)**. Although they are designed for the same 3-SAT instance, the hypergraph-based solver exhibits a more streamlined architecture. It involves only 8 vertices, each corresponding directly to one of the 8 literals and simultaneously serving as output terminals. The network has significantly fewer edges, totaling just 24, yet effectively captures all necessary relationships between the

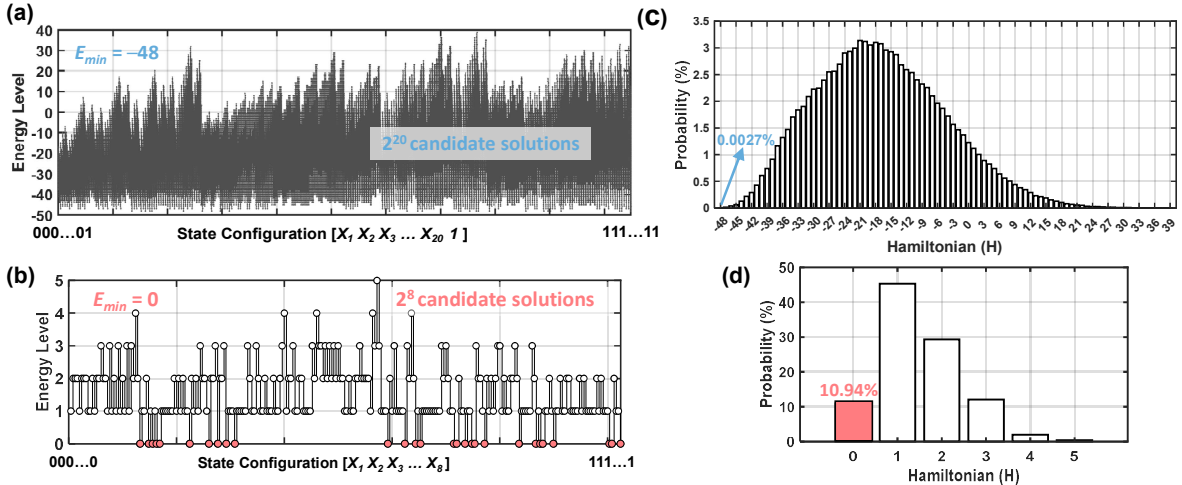


Fig. 5. Energy landscapes of 3-SAT solvers based on (a) the logic synthesis approach and (b) the hypergraph with direct mapping. Hamiltonian distributions of these two solvers based on (c) the logic synthesis approach and (d) the hypergraph with direct mapping.

variables (Fig. 4e). The structural differences between the two solver approaches lead to distinct energy landscapes. **Fig. 5(a)** illustrates the energy landscape of the conventional solver based on the merged SUGs. It spans a vast solution space of 2^{20} candidate configurations. The energy landscape of this solver is highly complex and chaotic, with energy levels fluctuating dramatically from -48 to 39 . The complexity of this energy landscape arises primarily from the differing energy level distributions associated with various types of IOR gates. Additionally, the energy band gaps, defined as the differences between the lowest energy level and the second lowest level, vary across these gates. Consequently, during logic synthesis, these mismatched energy levels accumulate and stack and finally lead to a rugged landscape characterized by numerous local minima.

In contrast, **Fig. 5(b)** shows the energy landscape of the hypergraph-based solver. The energy landscape is significantly simplified, with the solution space reduced to just 2^8 candidate configurations. Energy levels are discretized into clear, distinct bands, with the ground state $H_{total} = 0$ clearly visible and easily identifiable among the configurations. Compared to the logic synthesis approach, this direct mapping method allows for the direct design of the solver's energy landscape and its contribution is twofold. On one hand, the reduction in the number of vertices lowers the complexity of the energy landscape in terms of dimensionality. On the other hand, bypassing the stacking of energy levels helps to avoid the emergence of local minimum in the energy landscape, effectively reducing complexity in depth.

We then studied the Hamiltonian distribution of these two solvers in more detail. As shown in **Fig. 5(c)**, the energy landscape of the solver designed from the conventional approach, exhibits a more continuous and widely dispersed Hamiltonian distribution. The number of distinct energy levels N_{EL} for it is 88. In contrast, the hypergraph-based solver's landscape, shown in **Fig. 5(d)**, is more constrained. It exhibits fewer discrete energy levels with a range of $0\sim 5$, $N_{EL} = 6$, and a prominently distributed ground state. The ratio of the optimal solution corresponding to the ground state of the hypergraph-based solver to all candidate solutions is 4,052 times that of the conventional solver.

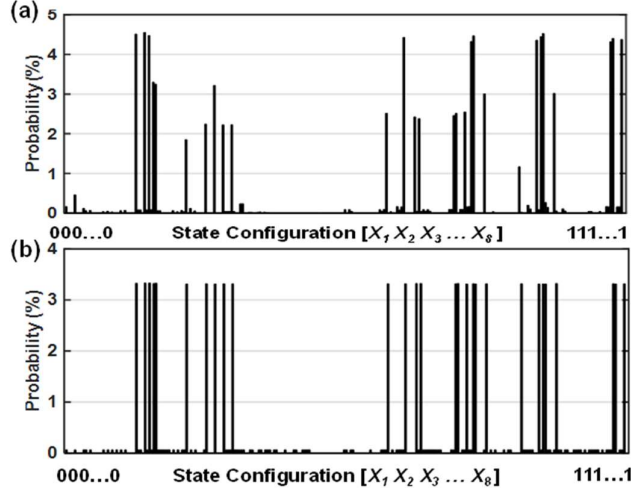


Fig. 6. Probability distributions of the solvers based on (a) the logic synthesis approach and (b) the hypergraph with direct mapping.

Further simulated experiments comparing the two solvers revealed distinct probability distributions for the given 8-literal and 12-clause 3-SAT problem instance. The two-body solver's results, shown in **Fig. 6(a)**, present a highly heterogeneous distribution. Sharp peaks with different heights represent valid solutions that are irregularly dispersed across the configuration space. This pattern suggests that the optimal solutions do not have a theoretically equal probability distribution. Instead, there are numerous local optima in this complex energy landscape. In contrast, the hypergraph-based solver's results, shown in **Fig. 6(b)**, exhibit a more uniform and structured pattern. The 28 optimal solutions, i.e. valid satisfying assignments, make the entire formula true, exhibit almost equiprobable states, represented as uniformly sized bars. This regular structure implies that the optimal solutions are mapped to the same ground state with $H_{total} = 0$ in the energy landscape.

More challenging instances from the SATLIB benchmark, specifically the uf20-91 problems—a 3-SAT formulation with 20 literals and 91 clauses—were studied. Simulated annealing was employed to evaluate the solver's performance in these complex instances. **Fig. 7(a)** illustrates the evolution of state configurations across 100 trials over 200 annealing cycles for the uf20-01 instance. The results indicate that the solver successfully identified 8 optimal solutions, which are highlighted by the pink solid box. **Fig. 7(b)** shows the corresponding changes in Hamiltonian values over the annealing process, where 99 out of 100 trials converged to the ground state, achieving the ground state with $H_{total} = 0$. The average number of annealing cycles required for convergence was 18.92. However, one trial, represented by the light blue line, failed to converge to the ground state and maintained a higher energy level of $H_{total} = 2$ throughout the annealing process.

The success rates of this 20-vertex hypergraph-based solver with the conventional 112-vertex SUG-based solver when applied to the uf20-01 instance are then compared in **Fig. 7(c)**. The proposed solver achieved a remarkably high success rate of 99%, significantly outperforming the conventional solver, which achieved only a 1% success rate. This substantial improvement

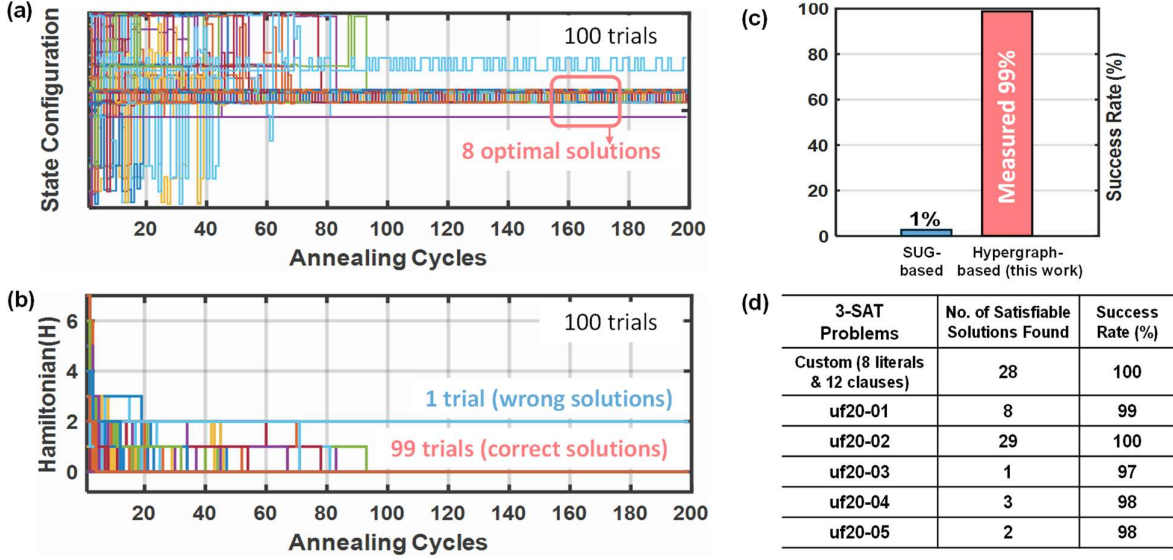


Fig. 7. 100 simulated experiments were conducted on the uf20-01 3-SAT instance from the SATLIB benchmark using the hypergraph-based solver under simulated annealing. (a) The evolution of the 20-vertex state configurations $[x_1, x_2, x_3, \dots, x_{20}]$ over annealing cycles. (b) corresponding energy changes in the system. A linear annealing schedule was adopted in this work. (c) Comparison of success rates for solving the uf20-01 3-SAT instance over 100 trials using the two solvers. (d) Number of satisfying solutions and corresponding success rates found by the hypergraph-based solver for custom 3-SAT instances and other instances from the uf20-91 files.

underscores the effectiveness of the hypergraph-based approach with direct mapping in navigating complex energy landscapes and finding optimal solutions efficiently.

A summary of the performance of the hypergraph-based solver across various instances of the uf20-91 problems is provided in **Fig. 7(d)**. The table details the number of satisfiable solutions found and the corresponding success rates for each instance. The results consistently demonstrate that the hypergraph-based solver not only identifies a higher number of satisfiable solutions but also maintains high success rates across different problem instances, which further affirms its scalability and robustness in solving large-scale 3-SAT problems.

Conclusion

This study introduces a hypergraph-based probabilistic computing framework that effectively addresses the limitations of traditional SAT solvers in handling large-scale 3-SAT problems. By employing a direct mapping from logical expressions to hypergraphs, our approach bypasses the unavoidable logic decomposition and synthesis procedures in conventional probabilistic SAT solvers. It significantly reduces the vertex count and connectivity complexity and achieves the theoretically minimum solution space. Simulation results show that the proposed approach has great benefits in improving the performance of probabilistic 3-SAT solvers. For example, in solving the uf20-01 instance, the proposed solver achieved a 99% success rate, compared to only 1% for the optimized logic synthesis-based solver, and required an average of 18.92 annealing cycles for convergence, which represents a substantial reduction in computational effort. Furthermore, the energy landscape of our hypergraph-based solver exhibited fewer local minima and more uniform

Hamiltonian distributions, leading to a more robust search for optimal solutions. These findings underscore the effectiveness of the hypergraph-based direct mapping approach in overcoming the scalability challenges posed by large-scale SAT problems and demonstrate its potential as a powerful tool for future research in probabilistic computing and combinatorial optimization.

Methods

BM-Based energy model

The physical mechanism underlying probabilistic 3-SAT solvers is rooted in the Boltzmann Law. Once the system's configuration i.e., the interconnection relationship, including bias terms, pairwise interaction terms and/or three-body interaction terms, is established, the energy of the system solely depends on the state of the nodes. The steady probability for each state configuration can then be described by the Boltzmann distribution:

$$P(\{x\}) = \frac{e^{-\alpha \cdot E(\{x\})}}{\sum_{\{x'\}} e^{-\alpha \cdot E(\{x'\})}} \quad (5)$$

where α represents a pseudo-temperature parameter indicating the stochasticity level of the system. The encoding of the solution into the ground state is essential in the process of solving the SAT problem, as configurations with the lowest energy are naturally favored during temporal evolution.

Simulated Annealing

To further enhance the solution convergence and optimize computational performance, we integrate a simulated annealing procedure into the solver. simulated annealing systematically modulates the pseudo-temperature parameter, increasing it gradually according to the relationship:

$$\alpha(t) = \alpha_0 + \beta t \quad (\beta > 0) \quad (6)$$

where α_0 is the initial inverse temperature and determines the annealing rate. Initially, with a relatively low α , the solver explores a broad range of state configurations, effectively escaping local minima. Over time, as α increases, stochastic fluctuations diminish, thereby sharpening the Boltzmann distribution around the states of lowest energy. Ultimately, as α approaches infinity, the probability distribution converges to the ground state, ensuring efficient and accurate identification of the optimal solution.

Acknowledgements

This work at the National University of Singapore was supported by FRC-A-8000194-01-00. G.C. L. would also like to thank the financial support from the National Science and Technology Council (NSTC) under grant number NSTC 112-2112-M-A49-047-MY3, the Co-creation Platform of the Industry-Academia Innovation School, NYCU, under the framework of the National Key Fields Industry-University Cooperation and Skilled Personnel Training Act, and the Advanced Semiconductor Technology Research Center from The Featured Areas Research Center Program within the framework of the Higher Education Sprout Project by the Ministry of Education (MOE) in Taiwan.

Data availability

The data that support the plots within this paper and the other findings of this study are available from the corresponding author upon reasonable request.

Code availability

The computer code and problem instances used in this study are available from the corresponding authors upon reasonable request.

Author contributions

H.Y. and L.G. conceptualized the study and proposed the idea of solving Boolean satisfiability problems with using the hypergraph-based method under the probabilistic computing paradigm. H.Y. designed and conducted simulation experiments with the help of Z.W. H.M. fabricated the p-bit device with help from S.C., L.H., H.Y.C, and W.J. H.Y., G.X, H.T., and L.G., analyzed the simulation and experimental data. H.Y. and H.M. drafted the manuscript with input from all other authors. All authors discussed the results and reviewed the manuscript.

Corresponding authors

Correspondence and requests for materials should be addressed to L.G. (Email: gcliang@nycu.edu.tw).

Competing interests

The authors declare no competing interests.

References

1. Singh, N. S. *et al.* CMOS plus stochastic nanomagnets enabling heterogeneous computers for probabilistic inference and learning. *Nat. Commun.* **15**, 2685 (2024).
2. Chowdhury, S. *et al.* A full-stack view of probabilistic computing with p-bits: devices, architectures and algorithms. *IEEE J. Explor. Solid-State Comput. Devices Circuits* 1–1 (2023) doi:10.1109/JXCDC.2023.3256981.
3. Aadit, N. A. *et al.* Massively parallel probabilistic computing with sparse Ising machines. *Nat. Electron.* **5**, 460–468 (2022).
4. Daniel, J. *et al.* Experimental demonstration of an on-chip p-bit core based on stochastic

- magnetic tunnel junctions and 2D MoS₂ transistors. *Nat. Commun.* **15**, 4098 (2024).
5. Cai, B. *et al.* Unconventional computing based on magnetic tunnel junction. *Appl. Phys. A* **129**, 236 (2023).
 6. Finocchio, G. *et al.* Roadmap for unconventional computing with nanotechnology. *Nano Futur.* **8**, 012001 (2024).
 7. Kaiser, J. & Datta, S. Probabilistic computing with p-bits. *Appl. Phys. Lett.* **119**, 150503 (2021).
 8. Cai, F. *et al.* Power-efficient combinatorial optimization using intrinsic noise in memristor Hopfield neural networks. *Nat. Electron.* **3**, 409–418 (2020).
 9. Mohseni, N., McMahon, P. L. & Byrnes, T. Ising machines as hardware solvers of combinatorial optimization problems. *Nat. Rev. Phys.* **4**, 363–379 (2022).
 10. Patel, S., Canoza, P. & Salahuddin, S. Logically synthesized and hardware-accelerated restricted Boltzmann machines for combinatorial optimization and integer factorization. *Nat. Electron.* **5**, 92–101 (2022).
 11. Lee, K., Chowdhury, S. & Camsari, K. Y. Noise-augmented Chaotic Ising Machines for Combinatorial Optimization and Sampling. Preprint at <http://arxiv.org/abs/2408.04744> (2024).
 12. Camsari, K. Y., Sutton, B. M. & Datta, S. p-bits for probabilistic spin logic. *Appl. Phys. Rev.* **6**, 011305 (2019).
 13. Camsari, K. Y., Faria, R., Sutton, B. M. & Datta, S. Stochastic p-bits for invertible logic. *Phys. Rev. X* **7**, 031014 (2017).
 14. Pervaiz, A. Z., Sutton, B. M., Ghantasala, L. A. & Camsari, K. Y. Weighted \$ p \\$-Bits for FPGA Implementation of Probabilistic Circuits. *IEEE Trans. Neural Netw. Learn. Syst.* **30**, 1920–1926 (2018).

15. Pervaiz, A. Z., Ghantasala, L. A., Camsari, K. Y. & Datta, S. Hardware emulation of stochastic p-bits for invertible logic. *Sci. Rep.* **7**, 10994 (2017).
16. Bybee, C. *et al.* Efficient optimization with higher-order ising machines. *Nat. Commun.* **14**, 6033 (2023).
17. Shim, Y., Jaiswal, A. & Roy, K. Ising computation based combinatorial optimization using spin-Hall effect (SHE) induced stochastic magnetization reversal. *J. Appl. Phys.* **121**, 193902 (2017).
18. Kim, J. *et al.* Fully CMOS-Based p-Bits with a Bistable Resistor for Probabilistic Computing. *Adv. Funct. Mater.* **34**, 2307935 (2024).
19. Vardi, M. Y. Boolean satisfiability: theory and engineering. *Commun. ACM* **57**, 5–5 (2014).
20. Littman, M. L., Majercik, S. M. & Pitassi, T. Stochastic Boolean Satisfiability. *J. Autom. Reason.* **27**, 251–296 (2001).
21. Marques-Silva, J. P. & Sakallah, K. A. Boolean satisfiability in electronic design automation. in *Proceedings of the 37th conference on Design automation - DAC '00* 675–680 (ACM Press, Los Angeles, California, United States, 2000). doi:10.1145/337292.337611.
22. Semenov, A. & Zaikin, O. Algorithm for finding partitionings of hard variants of boolean satisfiability problem with application to inversion of some cryptographic functions. *SpringerPlus* **5**, 554 (2016).
23. Aadit, N. A. *et al.* Massively parallel probabilistic computing with sparse Ising machines. *Nat. Electron.* **5**, 460–468 (2022).
24. Aadit, N. A. *et al.* Computing with invertible logic: Combinatorial optimization with probabilistic bits. in *2021 IEEE International Electron Devices Meeting (IEDM)* 40–3 (IEEE, 2021).

25. Grimaldi, A. *et al.* Spintronics-compatible Approach to Solving Maximum-Satisfiability Problems with Probabilistic Computing, Invertible Logic, and Parallel Tempering. *Phys. Rev. Appl.* **17**, 024052 (2022).
26. Onizawa, N. *et al.* A Design Framework for Invertible Logic. *IEEE Trans. Comput.-Aided Des. Integr. Circuits Syst.* **40**, 655–665 (2021).
27. He, Y., Luo, S., Fang, C. & Liang, G. Direct design of ground-state probabilistic logic using many-body interactions for probabilistic computing. *Sci. Rep.* **14**, 15076 (2024).
28. Pedretti, G. *et al.* Solving Boolean satisfiability problems with resistive content addressable memories. *Npj Unconv. Comput.* **2**, 7 (2025).
29. He, Y., Fang, C., Luo, S. & Liang, G. Many-Body Effects-Based Invertible Logic with a Simple Energy Landscape and High Accuracy. *IEEE J. Explor. Solid-State Comput. Devices Circuits* 1–1 (2023) doi:10.1109/JXCDC.2023.3320230.
30. Bashar, M. K. & Shukla, N. Designing Ising machines with higher order spin interactions and their application in solving combinatorial optimization. *Sci. Rep.* **13**, 9558 (2023).
31. Bashar, M. K., Mallick, A., Ghosh, A. W. & Shukla, N. Dynamical System-Based Computational Models for Solving Combinatorial Optimization on Hypergraphs. *IEEE J. Explor. Solid-State Comput. Devices Circuits* **9**, 21–28 (2023).
32. Su, Y., Kim, T. T.-H. & Kim, B. A Reconfigurable CMOS Ising Machine With Three-Body Spin Interactions for Solving Boolean Satisfiability With Direct Mapping. *IEEE Solid-State Circuits Lett.* **6**, 221–224 (2023).
33. Grimaldi, A., Raimondo, E., Giordano, A., Çamsarı, K. Y. & Finocchio, G. A Comparison of Energy Minimization Algorithms for Solving Max-Sat Problem with Probabilistic Ising

- Machines. in *2023 IEEE 23rd International Conference on Nanotechnology (NANO)* 698–702 (IEEE, Jeju City, Korea, Republic of, 2023). doi:10.1109/NANO58406.2023.10231311.
34. Smithson, S. C., Onizawa, N., Meyer, B. H., Gross, W. J. & Hanyu, T. Efficient CMOS invertible logic using stochastic computing. *IEEE Trans. Circuits Syst. Regul. Pap.* **66**, 2263–2274 (2019).
35. Camsari, K. Y., Salahuddin, S. & Datta, S. Implementing p-bits With Embedded MTJ. *IEEE Electron Device Lett.* **38**, 1767–1770 (2017).
36. Safranski, C. *et al.* Demonstration of Nanosecond Operation in Stochastic Magnetic Tunnel Junctions. *Nano Lett.* **21**, 2040–2045 (2021).
37. Woo, K. S. *et al.* Probabilistic computing using Cu0.1Te0.9/HfO2/Pt diffusive memristors. *Nat. Commun.* **13**, 5762 (2022).
38. Wang, K. *et al.* Threshold switching memristor-based stochastic neurons for probabilistic computing. *Mater. Horiz.* **8**, 619–629 (2021).
39. Aadit, N. A., Mohseni, M. & Camsari, K. Y. Accelerating Adaptive Parallel Tempering with FPGA-based p-bits. in *2023 IEEE Symposium on VLSI Technology and Circuits (VLSI Technology and Circuits)* 1–2 (IEEE, Kyoto, Japan, 2023). doi:10.23919/VLSITechnologyandCir57934.2023.10185207.
40. Luo, S., He, Y., Cai, B., Gong, X. & Liang, G. Probabilistic-Bits Based on Ferroelectric Field-Effect Transistors for Probabilistic Computing. *IEEE Electron Device Lett.* **44**, 1356–1359 (2023).
41. Wu, M.-H. *et al.* Compact Probabilistic Poisson Neuron Based on Back-Hopping Oscillation in STT-MRAM for All-Spin Deep Spiking Neural Network. in *2020 IEEE Symposium on VLSI*

Technology 1–2 (IEEE, Honolulu, HI, USA, 2020).

doi:10.1109/VLSITechnology18217.2020.9265033.